applied optics

Relationship analysis between transient thermal control mode and image quality for an aerial camera

Weiyi Liu,* Yongsen Xu, Yuan Yao, Yulei Xu, Honghai Shen, and Yalin Ding

Key Laboratory of Airborne Optical Imaging and Measurement, Changchun Institute of Optics, Fine Mechanics and Physics, Chinese Academy of Sciences, Changchun 130033, China
**Corresponding author: 2219101@163.com*

Received 26 May 2016; revised 11 October 2016; accepted 25 November 2016; posted 4 January 2017 (Doc. ID 267116); published 27 January 2017

Thermal control and temperature uniformity are important factors for aerial cameras. This paper describes the problems with existing systems and introduces modifications. The modifications have improved the temperature uniformity from 12.8°C to 4.5°C, and they enable images to be obtained at atmospheric and low pressures (35.4 KPa). First, thermal optical analysis of the camera is performed by using the finite element analysis method. This modeled the effect of temperature level and temperature gradient on imaging. Based on the results of the analysis, the corresponding improvements to the thermal control measures are implemented to improve the temperature uniformity. The relationship between the temperature control mode and temperature uniformity is analyzed. The improved temperature field corresponding to the thermal optical analysis is studied. Taking into account that the convection will be affected by the low pressure, the paper analyzes the thermal control effect, and imaging results are obtained in low pressure. The experimental results corroborate the analyses.

OCIS codes: (120.6780) Temperature; (120.6810) Thermal effects; (040.1490) Cameras; (110.2960) Image analysis.

https://doi.org/10.1364/AO.56.001028

1. INTRODUCTION

The performance of aerial cameras is closely related to thermal control devices [1–3]. Compared to the ground environment, the aerial camera operates in an atmospheric environment which is considerably worse. The worsening atmospheric conditions decrease the camera's performance or even stop it from working properly. Therefore, effective and reliable thermal control measures are indispensable in order to obtain high-precision and high-resolution images [4]. Owing to the increasing requirements on focal length and resolution, aerial cameras have to raise their requirements on temperature: it has become inevitable for aerial cameras to carry thermal control devices. In recent years, the thermal control technique in space has become relatively mature. The developed thermal control device has stronger control ability, higher precision, and stronger adaptability, which is also useful in the design of aerial cameras [5–9]. However, this does not imply that all of the thermal control devices can be used in aerial cameras [10–12]. The thermal control devices for aerial cameras must consider both temperature level and temperature uniformity during the transient change process, otherwise it will affect the imaging quality. This paper discusses the problems arising from the original thermal control, analyzes the cause of the problem, and shows the importance of temperature uniformity. The paper analyzes the impact of the existing temperature control measures on temperature uniformity under transient conditions. Finally, a set of thermal control measures are modified to meet the camera's demand for temperature control.

2. EXPERIMENTAL PHENOMENA OF AN AERIAL CAMERA

The camera is a CCD visible light camera. It is used in aviation, working in the high altitude of the cold environment. Its focal length is 1.5 m, which is very sensitive to temperature.

To adapt to the cold environment of aviation, a thermal control system was implemented in the aerial camera. The system consisted of heating films, temperature sensors, and temperature control boards. The heating films were attached to thin-walled components; the temperature sensors measured the temperatures and provided feedback; the temperature control boards controlled the heating temperature of the films based on the feedback. When the measured temperature was lower than the target, the film heated; when the measured temperature was higher than the target, the film stopped heating.

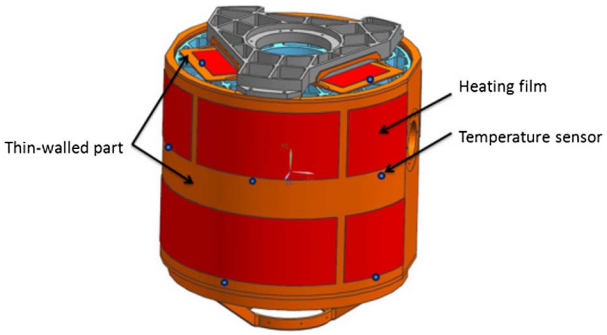

Fig. 1. Heating film and temperature sensor.

Table 1. Distribution and Power of the Heating Film

Distribution	Size (mm)	Number	Power (W)
Primary mirror holder	100 × 40	3	15
Secondary mirror holder	Φ80	1	20
Main tube (X axis)	600 × 100	4	60
Main tube (Y axis)	100 × 100	8	32

The heating film was uniformly attached to the thin wall, and the temperature sensor was attached to the edge of the films, as shown in Fig. 1. Table 1 shows the distribution and power of the heating film.

During the ground test, it was found that the low temperature environment reduced the quality of the camera's image. The specific test procedure was as follows: the camera (initial temperature 20°C) was placed in a −30°C aviation environment simulation chamber. Using the reflector at the bottom of the chamber, the camera photographed the target on the collimator 10 m away from the reflector, as shown in Fig. 2. The camera began to cool down due to the external environment. When the temperature was below 20°C, the thermal control system began to work and maintained all temperature sensors at the temperature level of 20°C. Table 2 reports the temperature of each point in the camera. The data in Table 2 shows that the measured temperature was within the desired range. However, the image quality of the target was not ideal when the thermal control system was on. When the thermal control system was shut down, the image quality improved, indicating a

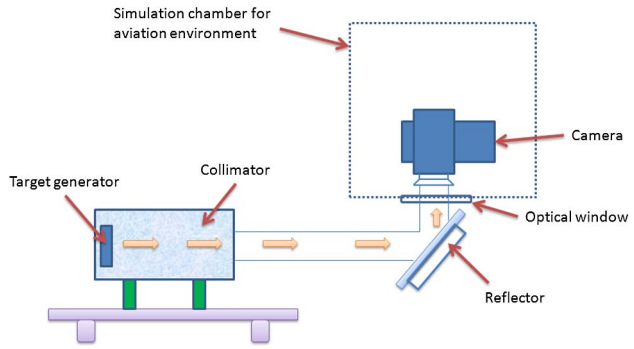

Fig. 2. Layout of the experimental device on the ground simulation test.

Table 2. Temperature of Each Point Under the Original Thermal Control Condition

Sensor Location	Temperature (°C)
Primary mirror	19.3
Secondary mirror	18.2
Third mirror	19.8
Primary mirror holder	20.3
Secondary mirror holder	20.1
Lens barrel	21.3

negative role of the thermal control system in the photographic process.

Figure 3, which shows the target, confirms the above conjecture. The three images of Fig. 3 are obtained under different conditions for the same target, which consists of 25 sets of black and white stripes of different widths between 10 μm and 40 μm, with each set including four different orientations. The imaging effect is judged by distinguishing the stripes. Figure 3(a) shows an image obtained by the camera under the design temperature conditions (20°C±2°C). At the bottom of the figure, from left to right, are groups 1 to 5. On the right-hand side, from bottom to top, are groups 5 to 9. The group numbers in the figure are reversed, and the 3rd and 7th groups are not marked. In Fig. 3(a), the direction of the set of stripes in group 7 can be distinguished. (The index requirement is to distinguish the direction of the stripes in the 5th group). Figure 3(b) was obtained with the camera in the aviation environment simulation chamber of −30°C after the thermal

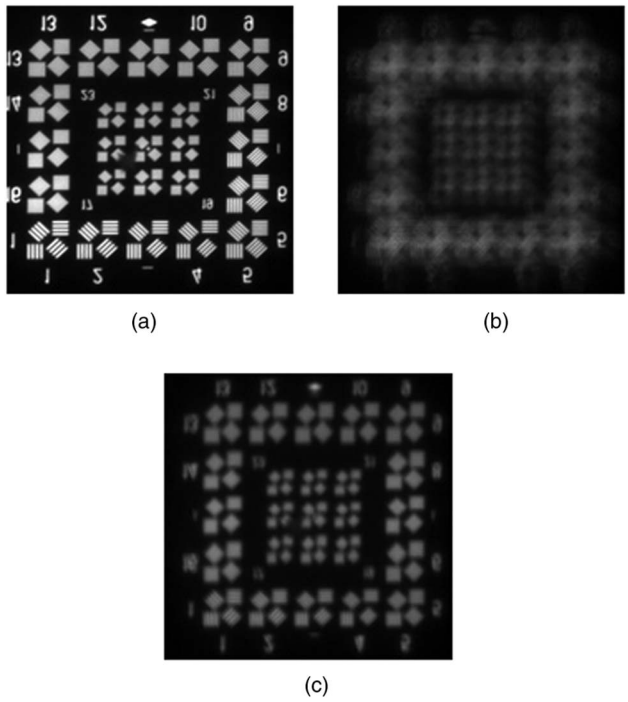

Fig. 3. Images of target under different conditions. (a) Design temperature condition. (b) At low temperatures with original thermal control. (c) At low temperatures without thermal control.

control system had been running for 40 min. The image quality is very poor and none of the set of stripes can be resolved. Figure 3(c) was obtained after the thermal control system was shut down and the camera cooled down for 20 min in the chamber. The direction of the 2nd group of stripes could just about be determined. The image quality is not as good as in Fig. 3(a), but better than that in Fig. 3(b).

3. IMAGING PHENOMENON ANALYSIS

Although all of the test temperature levels are within the design range, the image is still blurry [Fig. 3(b)]. This is due to uneven temperature.

A. Influence of Temperature Level and Temperature Gradient on Imaging

Researching temperature effects on imaging systems involves a number of subjects, such as mechanics, thermotics, and optics. For an optical device used for imaging, a temperature change will affect its surface shapes and its refractive index. For the support structure which does not directly participate in imaging, the change of temperature will make its shape change, and at the same time generate stress acting on the optical devices, hence causing a change in the strain of the optical device, in its position, and its surface shape. All of these will affect the imaging process [13].

In order to analyze these effects, the system needs to be analyzed by using thermal optics [14]. The process can be outlined as follows. (1) Establish the finite element mechanical model for the whole system; (2) import the temperature level and temperature gradient and analyze changes of stress and displacement of each node under the conditions; (3) bring the changes of surface shape and refractive index involved in imaging into the optical model after some corresponding conversions; and (4) analyze their influence on imaging.

In this system, a temperature level difference of 20°C (design temperature is 20°C and a field temperature of 0°C is adopted) and a temperature gradient (axial temperature difference) of 20°C are used. After finite element modeling and mechanical analysis (by using software NX-nastran), the nodal displacement of the optical surface is brought into the optical analysis software (CODE V) for optical analysis. Third-order aberrations of the system are obtained under two temperature fields, respectively. The analysis results are shown in Table 3. Table 3(a) shows the effect of temperature level difference (0°C) on the system. Each line represents an optical surface; the first three lines are the main mirror, secondary mirror, and third mirror, respectively. The secondary mirror is an aperture stop. The next 10 lines are the optical surfaces of the redressing lens in the lens barrel. The last line of data contains the third-order aberrations produced by the superposition of all the surfaces of the system. SA, TCO, TAS, and SAS represent spherical aberration, coma, meridional image power, and sagittal image power, respectively. From these data it can be seen that the main sources of aberration are the primary mirror and the secondary mirror. The system is affected by spherical aberration and a small amount of coma (shown by the Seidel coefficient numbers in the red box, −2.62 and 0.42, respectively). Table 3(b) shows the effect of temperature gradient on the system. The system has spherical aberration and coma (−2.62 and 1.64, respectively). Therefore, changes in temperature level and temperature gradient will both introduce spherical aberration to the system, while changes in temperature gradient will additionally introduce significant amounts of coma. The system has an auto-focus function which can partially compensate for the spherical aberration; however, this does not improve coma. Therefore, the level of coma determines the imaging quality of the system. This means that the system is more sensitive to changes in temperature gradient than in the temperature level. Table 3 compares the effect of temperature level difference and temperature gradient on the optical system, and the main difference is in the coma (TCO).

Table 3. Analysis of Third-Order Aberrations

	SA	TCO	TAS	SAS
(a) Temperature level difference of 20°C				
1	−5.097138	0.835460	−0.040494	−0.010064
STO	2.477660	−0.426739	0.016333	0.000000
3	0.059987	−0.022638	0.002609	0.000711
4	0.016421	0.007955	0.001457	0.000601
5	0.050710	0.099392	0.074688	0.031396
6	−0.018237	−0.048523	−0.048741	−0.020051
7	−0.239838	−0.164970	−0.043400	−0.018184
8	0.003780	0.018761	0.021384	0.000694
9	−0.005835	0.015879	−0.007361	0.002242
10	0.141540	0.087551	0.021507	0.009472
11	−0.005124	0.013477	−0.007936	−0.000059
12	0.015776	−0.010174	0.002187	0.000729
13	−0.015437	0.009955	−0.002140	−0.000713
SUM	−2.615735	0.415387	−0.009907	−0.003226
(b) Temperature gradient of 20°C				
1	−5.097138	3.302527	−0.632756	−0.157252
STO	2.477660	−1.686876	0.255219	0.000000
3	0.059987	−0.089486	0.040768	0.011103
4	0.016421	0.031444	0.022769	0.009390
5	0.050710	0.392892	1.167054	0.490591
6	−0.018237	−0.191807	−0.761613	−0.313311
7	−0.239838	−0.652115	−0.678163	−0.284143
8	0.003780	0.074160	0.334146	0.010847
9	−0.005835	0.062769	−0.115021	0.035028
10	0.141540	0.346086	0.336063	0.148012
11	−0.005124	0.053273	−0.124013	−0.000920
12	0.015776	−0.040217	0.034175	0.011392
13	−0.015437	0.039352	−0.033440	−0.011147
SUM	−2.615735	1.642001	−0.154811	−0.050412

B. Analysis of the Transient Temperature Field for the Camera

Based on the camera's finite element thermal model, the simulation analysis has been done according to the existing conditions of thermal control. The transient thermal analysis considers the factors of conduction, convection, and radiation. Figure 4 shows the temperature distribution after 40 min. The temperature values are on the right side, and the unit is °C. It can be seen from the numerals that the temperature distribution is not uniform. The maximum temperature is 21.5°C, the minimum temperature is 8.7°C, and the maximum temperature difference is 12.8°C. The temperature inhomogeneity is mainly concentrated in the main tube and lens barrel. Table 4 is the theoretical analysis of the temperature of each

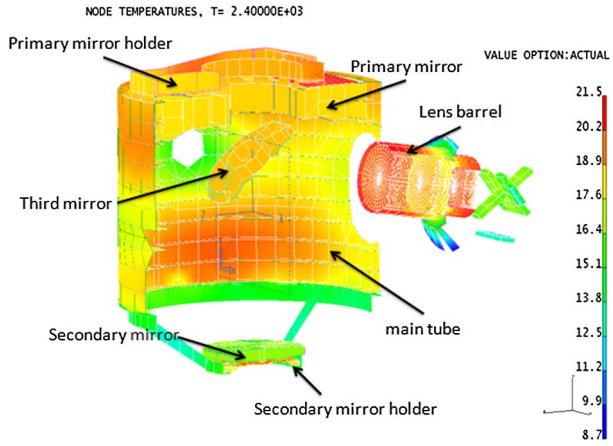

Fig. 4. Analysis of temperature distribution at 40 min. Right: Values in degrees Celsius.

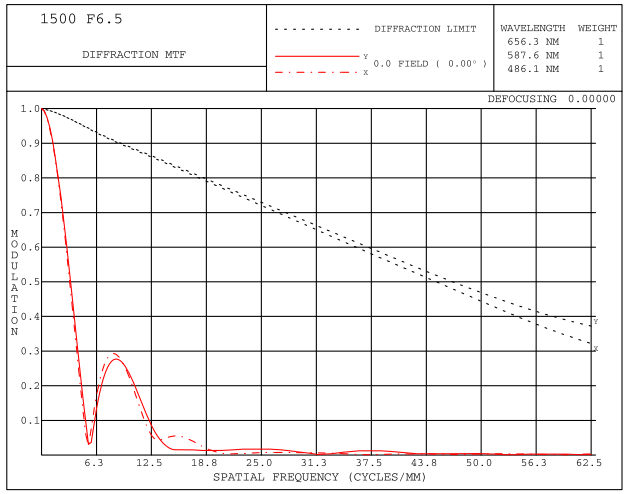

Fig. 5. MTF in original thermal control state.

Table 4. Analyzed Temperature of Each Point

Sensor Location	Analytical Temperature (°C)
Primary mirror	19.0
Secondary mirror	17.6
Third mirror	19.7
Primary mirror holder	20.1
Secondary mirror holder	20.7
Lens barrel	21.4

point in the camera; the data here show little difference from the actual test results in Table 2. The data in Table 4 in Table 2. It can be seen that there is between them. Thus it can be seen that although the values of the temperature sensors are all at about 20°C, the overall system temperature is not uniform. Table 5 and Fig. 5 show the third-order aberration analysis and MTF in this state, respectively. It can be seen that aberrations are mainly generated by the primary mirror and the secondary mirror (the 1st line and 2nd line). Spherical aberration and coma are the most significant third-order aberrations in the system. According to the finite element analysis, the temperature level changes will cause the main tube expansion or contraction, thus causing changes of relative distance between the main mirror and second mirror, which can cause spherical aberration. The temperature gradient will cause deformation of the main tube itself, leading to a relative change of distance and tilt between the primary mirror and secondary mirror, which are connected via the main tube. This produces spherical aberration and coma. Coma cannot be compensated for by the system. Therefore, the inhomogeneity of the temperature affects the camera's imaging. Table 5 and Fig. 5 show the system's three order aberrations and MTF under the condition of obtaining Fig. 3(b), respectively. Because of the uneven temperature, the system produces a corresponding amount of spherical aberration and coma which cannot be compensated for.

Table 5. Third-Order Aberration Analysis in Original Thermal Control State

	SA	TCO	TAS	SAS
1	−5.097138	1.981388	−0.227762	−0.056603
STO	2.477660	−1.012060	0.091867	0.000000
3	0.059987	−0.053688	0.014675	0.003997
4	0.016421	0.018865	0.008196	0.003380
5	0.050710	0.235720	0.420085	0.176590
6	−0.018237	−0.115077	−0.274145	−0.112777
7	−0.239838	−0.391244	−0.244107	−0.102278
8	0.003780	0.044493	0.120277	0.003904
9	−0.005835	0.037659	−0.041402	0.012608
10	0.141540	0.207638	0.120967	0.053277
11	−0.005124	0.031962	−0.044639	−0.000331
12	0.015776	−0.024129	0.012301	0.004100
13	−0.015437	0.023610	−0.012037	−0.004012
SUM	−2.615735	0.985136	−0.055725	−0.018146

4. RELATIONSHIP BETWEEN TEMPERATURE CONTROL MODE AND TEMPERATURE UNIFORMITY

This section focuses on the relationship between temperature uniformity and two common aviation thermal control modes in the transient process.

A. Changing Temperature by Heating Films on the Thin Wall Plate

A heating film is attached to a thin wall plate. For a given target heating temperature, the film heats when the heating zone's temperature is below the target; the film stops heating when the temperature reaches the target. Temperature sensors provide feedback.

When the plate is heated, it can be considered isothermal along the direction of its thickness and the heating film area has a uniform heat flow. By ignoring the effects of convection and radiation, the system can be regarded as a two-dimensional unstable heat transfer process. If the film edge is adiabatic, the temperature of the entire area will increase uniformly. No temperature difference will occur. In practice, however, the film edge will never be adiabatic (for example, the heating area is not fully covered by the thin wall plate). Heat flow and heat

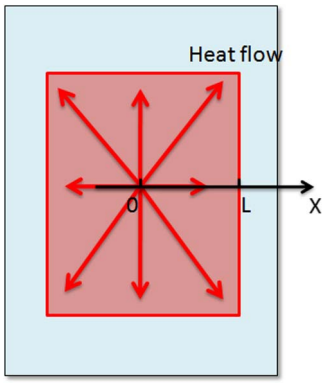

Fig. 6. Heat flow diagram of heating film.

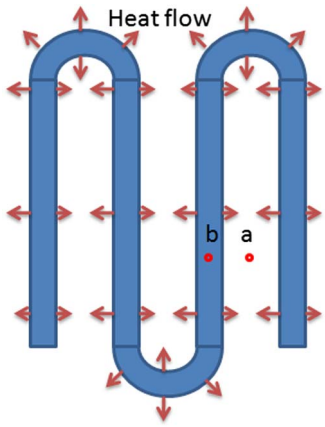

Fig. 7. Heat flow diagram of fluid convection.

loss are always present, that is heat will flow to the outer edge. In the entire system, heat will radically flow from the center of the heating zone to the periphery as shown in Fig. 6.

During the heating process, there will be temperature differences between the central region and the edge that can be analyzed by the micro-element method. Since the entire region is symmetrical, the analysis is illustrated in one direction. Suppose that a coordinate is set up with the center point being the origin and the edge point denoted as point L. The heat flows from the point of origin to the edge points. According to the relationship between the thermal resistance and heat flow, the temperature difference between the center and the edge region can be expressed as [15]

$$\Delta T = \frac{1}{k \cdot A} \int_0^L q_x \cdot \mathrm{d}x, \tag{1}$$

where ΔT is the temperature difference; q_x is the heat flow in the axial direction of the segment dx; k is the material's heat transfer coefficient; and A is plate's cross-sectional area perpendicular to the axial direction.

Equation (1) shows that the temperature difference is associated with the following factors: (a) the distance between the center and the edge, (b) heating power (heat flow), and (c) the thin wall plate's heat transfer coefficient. For example, when the heating film of the same size is attached to a Titanium Alloy plate (TC4, with the size 200 mm × 200 mm and a wall thickness of 5 mm), with a heating power of 50 W, the temperature difference between the center and the edge can reach 4°C–5°C in the heating transient process. The following measures can be adopted to reduce the temperature difference: (a) decrease the distance from the edge to the center by reducing the size of the heating film; this can be achieved by splitting the large heating film into several small pieces and controlling them individually; (b) reduce the power of the heating film; and (c) increase the heat transfer coefficient of the thin wall plate.

B. Changing Temperature by Fluid Circulation's Convection

The fluid's convection heat transfer consists of liquid convection and gas convection. Liquid has a stronger capacity of convection heat transfer and is often associated with denser pipeline systems. It can be used in places with large amount of heat (such as CCD, high density electronic devices, etc.)

As shown in Fig. 7, it is assumed that the pipes through which the liquid flows are evenly arranged on the thin wall plate. The thin wall plate can be considered isothermal along the direction of its thickness. Convection is generated between the liquid and the pipes. The pipes and thin wall plate exchange heat by conduction. Since the liquid is usually enclosed and circulating and the terminal will ensure a constant temperature for the liquid, the temperature of the liquid can be considered to be constant throughout the process. In the transient heat transfer process, the maximum temperature difference of the thin wall plate occurs between points a and b. Equation (1) is still applicable in this case. Therefore, in the process of changing temperature, the temperature difference is associated with the following factors: (a) the distance between a and b; (b) the convection heat transfer capability (heat flow in the formula); and (c) the heat transfer coefficient of the thin wall plate. The following measures can be adopted to reduce the temperature difference: (a) a denser arrangement of the piping system (increasing the convection heat transfer area); (b) a lower convection heat transfer capability; and (c) a higher heat transfer coefficient of the thin wall plate. Gas convection is usually performed in the whole cavity. Compared to liquid convection, it usually has a larger area of convection and relatively weak exchange capacity. Thus, gas convection has better temperature uniformity.

5. IMPROVEMENT OF THERMAL CONTROL MEASURES

Temperature uniformity plays a very important role in imaging by aerial remote sensors. This section makes some corrections based on the original thermal control system which could meet the demand of imaging. According to Section 4, the corrections are as follows.

(a) Reduce the power of each piece of heating film (using the PID control mode to reduce the power down to 50%), which therefore increases the temperature uniformity of the heating area during the transient heating period;
(b) increase several small convection thermal control devices in different areas of the camera. This can change the original natural convection into forced convection, and hence increase the temperature uniformity; and

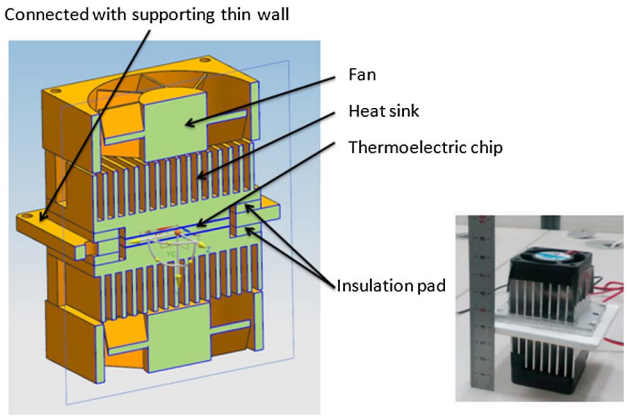

Fig. 8. Composition diagram of the device.

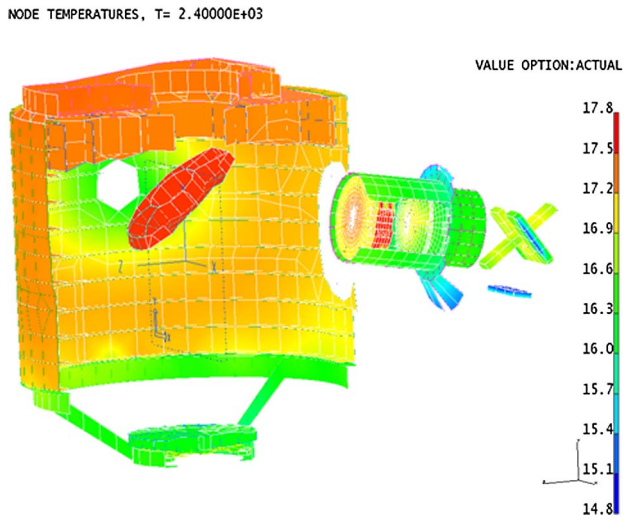

Fig. 9. Temperature distribution after modified thermal control measures. As can be seen from the temperature value on the right side, the temperature distribution is relatively uniform; the maximum temperature difference is 3°C.

(c) increase the outer insulation layer, which can reduce the impact of the external environment.

A. Small Convection Thermal Control Devices

The device uses a thermoelectric chip as the core and achieves the heat transfer by air convection. As shown in Fig. 8, the device consists of a thermoelectric chip, insulation pads, heat sinks, and fans. The device is vertically symmetrical. The thermoelectric chip is in the center of the device, with a fan at both ends. The middle edge is connected to the outer wall of the camera. The thermoelectric chip generates hot and cold ends due to the Pelletier effect. Both ends are connected to heat sinks. Fans are used to enhance the surrounding convection. The direction of the current can be changed to swap the cold and hot sides, allowing a dual function of heating or cooling the target. Table 6 shows the parameters of the thermoelectric chip and fan. A total of five devices are added inside the camera. They work together with the heating film. Two are arranged around the main tube to ensure the main optical system's uniform temperature, one is arranged around the lens barrel to meet the demand of temperature uniformity, and the other two are arranged in the outer frame to improve the temperature distribution of the camera body, providing a better environment for the optical system.

B. Temperature Field and Third-Order Aberrations After the Corrections of Thermal Control Measures

The thermal input and thermal boundary conditions are adjusted according to the thermal control measures' corrections. The rest of the thermal boundary conditions are the same as in Section 3.B. Transient thermal analysis is then carried out on the camera. Figure 9 shows the temperature distribution: the maximum temperature is 17.8°C, the minimum temperature is 14.8°C, and the maximum temperature difference is 3.0°C. After thermal optical analysis, the third-order aberrations for the system and MTF have been obtained at this state. The results of the analysis are shown in Table 7 and Fig. 10, showing that coma has decreased. Table 7 and Fig. 10 show the system's three order aberrations and MTF under the condition of modified thermal control measures, respectively. The coma has correspondingly reduced. The MTF can achieve a relative ideal state through focusing.

Table 6. Parameters of the Thermoelectric Chip and Fan

	Fan	Thermoelectric Chip
Rated Voltage (V)	12	12
Operating Voltage (V)	7 ~ 13.8	8.6 ~ 15.4
Rated Current (A)	0.1	2.1
Max. Airflow (CFM)	8.0	—
Power (W)	1.2	25.2
Size(mm)	40 × 40 × 28	30 × 30 × 4

C. Experimental Verification

The imaging effect of the camera with the modified thermal control system as described in Section 5.B has been verified experimentally. The camera was placed in the −30°C environment, and then the thermal control system operated for 40 min. The image was obtained and shown in Fig. 11(b). The direction of the 5th group of lines can be resolved. This proves the

Table 7. Third-Order Aberration Analysis After Modified Thermal Control Measures

	SA	TCO	TAS	SAS
1	−5.097138	0.264176	−0.004049	−0.001006
STO	2.477660	−0.134936	0.001633	0.000000
3	0.059987	−0.007158	0.000261	0.000071
4	0.016421	0.002515	0.000146	0.000060
5	0.050710	0.031428	0.007468	0.003139
6	−0.018237	−0.015343	−0.004873	−0.002005
7	−0.239838	−0.052164	−0.004339	−0.001818
8	0.003780	0.005932	0.002138	0.000069
9	−0.005835	0.005021	−0.000736	0.000224
10	0.141540	0.027684	0.002150	0.000947
11	−0.005124	0.004261	−0.000794	−0.000006
12	0.015776	−0.003217	0.000219	0.000073
13	−0.015437	0.003148	−0.000214	−0.000071
SUM	−2.615735	0.131347	−0.000991	−0.000323

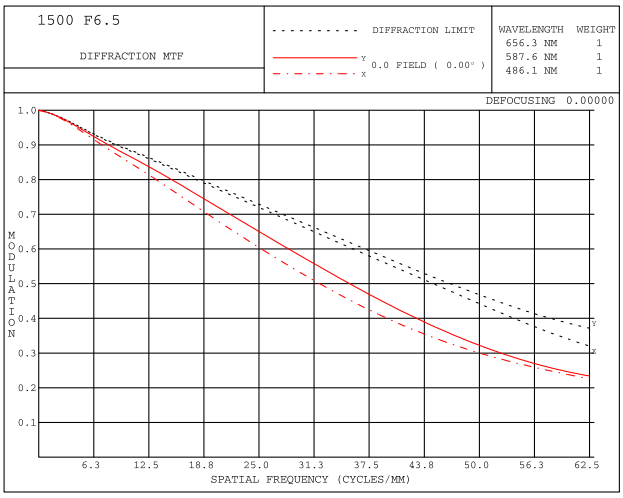

Fig. 10. MTF after modified thermal control measures.

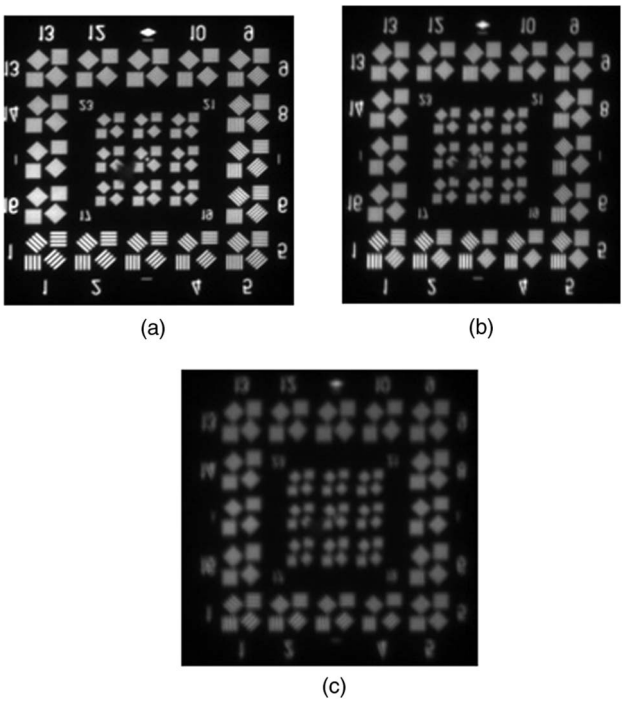

Fig. 11. Image under the condition of improved thermal control system. (a) Design temperature condition. (b) At low temperatures with new thermal control. (c) At low temperatures without thermal control.

effectiveness of the improved thermal control system. It can be seen that the new thermal control system has played a good role in imaging from the comparison between Figs. 11(b) and 11(c).

6. RELATIONSHIP BETWEEN PRESSURE CHANGES AND CONVECTION HEAT TRANSFER CAPABILITY

Aerial remote sensors work at a high altitude. The atmospheric pressure decreases with increasing height. If the remote sensor is not sealed, the internal pressure will decrease, which lowers the convection heat transfer capacity.

A. Analysis of the Convection Heat Transfer Capacity

The degree of weakened convection due to falling pressure could be measured by the convection heat transfer coefficient.

For both laminar and turbulent flow, the convection heat transfer coefficient can be expressed as [15]

$$h = \frac{k_f}{l} \cdot \mathrm{Nu}, \tag{2}$$

where k_f is the conductivity, l is convection length, and Nu is the Nusselt coefficient.

The Nusselt coefficient is a function of the Prandtl number and the Reynolds number. The Prandtl number of air is usually about 0.7 and can be approximately regarded as a constant. Then the Nusselt number is only a function of the Reynolds number. Most of the internal and external flow's heat transfer can expressed as [15]

$$\mathrm{Nu} = C_1(\mathrm{Re})^n, \tag{3}$$

where C_1 is a constant,

$$h = \frac{k_f}{l}\mathrm{Nu} = C_1 \frac{k_f}{l}\left(\frac{\rho u l}{\mu}\right)^n, \tag{4}$$

where u is speed, ν is kinematic viscosity, μ is dynamic viscosity, and ρ is density. n varies between 0.5 and 0.8. Dynamic viscosity μ and thermal conductivity k_f of air are mainly related to temperature.

For the ideal gas,

$$pV = R_g T, \tag{5}$$

where R_g is the gas constant, R is molar gas constant value, $R = 8.314$, M is gas molar mass, p is pressure, T is temperature, and V is specific volume, which is the reciprocal of density ρ. From Eq. (5):

$$\rho = \frac{p}{R_g T}. \tag{6}$$

If only pressure changes in the convection process, with temperature and speed unchanged, Eqs. (4)–(6) result in

$$\frac{h_1}{h_2} = \left(\frac{p_1}{p_2}\right)^n. \tag{7}$$

If the original pressure p_1 drops to p_2, let $P = \frac{p_2}{p_1}$ and the convection heat transfer coefficient ratio $H = \frac{h_2}{h_1}$. Equation (7) provides the relationship between the pressure ratio and the convection heat transfer coefficient ratio. Owing to different degrees of laminar flow or turbulent flow, n has a different range. The shaded area in Fig. 12 represents this relationship.

Figure 12 shows that the convection heat transfer coefficient decreases with pressure but at a slower rate compared to the reduction of pressure.

For example, the pressure at the altitude of 8 km is reduced to 35.1% of the original pressure on the ground, but the convection heat transfer capability decreases to about 43.3%–59.2% of the original level on the ground.

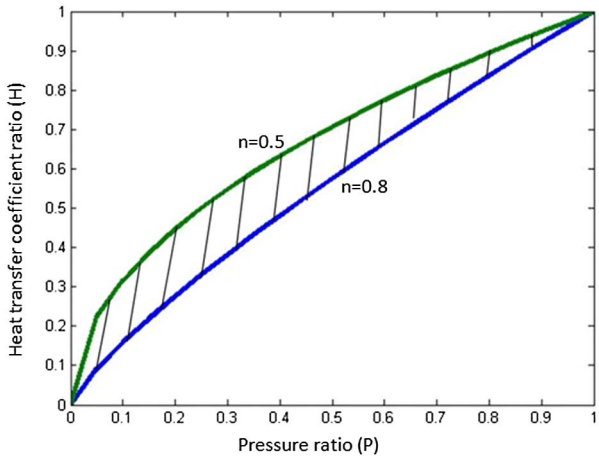

Fig. 12. Relationship diagram of pressure ratio and heat transfer coefficient ratio.

B. Temperature Field and Third-Order Aberration in Low Pressure

The thermal boundary conditions are the same as those in Section 3.B, except that the pressure is 35.1% of atmospheric pressure (35.4 KPa). The temperature field of the camera is obtained by the finite element thermal analysis method. Figure 13 shows the temperature distribution at 40 min. The maximum temperature is 18.4°C, the minimum temperature is 13.9°C, and the maximum temperature difference is 4.5°C. The third-order aberration analysis results and MTF are shown in Table 8 and Fig. 14, respectively. Table 8 and Fig. 14 show the system's three order aberrations and MTF with new thermal control measures under the condition of low pressure, respectively. The coma is slightly larger than in Table 7 and the MTF's value is slightly less than in Fig. 10 at 62.5 lp/mm.

C. Imaging Verification at Low Pressure

The experiment is carried out according to the conditions in Section 5.C. Figures 15(a) and 15(b) show images obtained under the conditions of normal pressure and low pressure, respectively. They are both relatively clear. It can be concluded that low pressure has little effect on the image quality under these conditions.

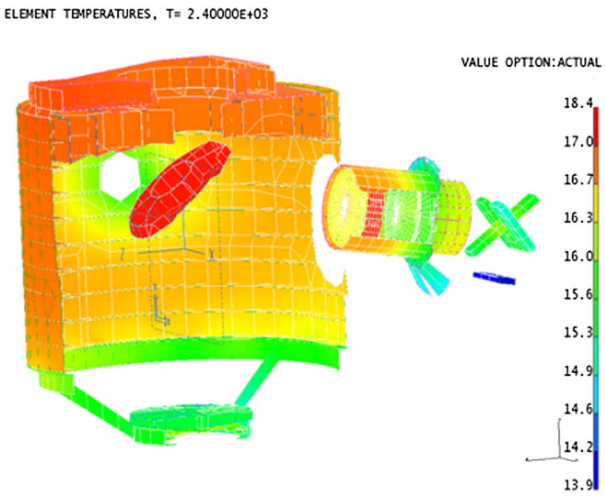

Fig. 13. Temperature distribution at 40 min with low pressure. The maximum temperature difference is 4.5°C. It is larger than in normal pressure (3.0°C).

Table 8. Third-Order Aberration with Low Pressure

	SA	TCO	TAS	SAS
1	−5.097138	0.330220	−0.006326	−0.001572
STO	2.477660	−0.168671	0.002552	0.000000
3	0.059987	−0.008948	0.000408	0.000111
4	0.016421	0.003144	0.000228	0.000094
5	0.050710	0.039285	0.011668	0.004905
6	−0.018237	−0.019179	−0.007615	−0.003132
7	−0.239838	−0.065205	−0.006780	−0.002841
8	0.003780	0.007415	0.003341	0.000108
9	−0.005835	0.006276	−0.001150	0.000350
10	0.141540	0.034605	0.003360	0.001480
11	−0.005124	0.005327	−0.001240	−0.000009
12	0.015776	−0.004021	0.000342	0.000114
13	−0.015437	0.003935	−0.000334	−0.000111
SUM	−2.615735	0.164184	−0.001548	−0.000504

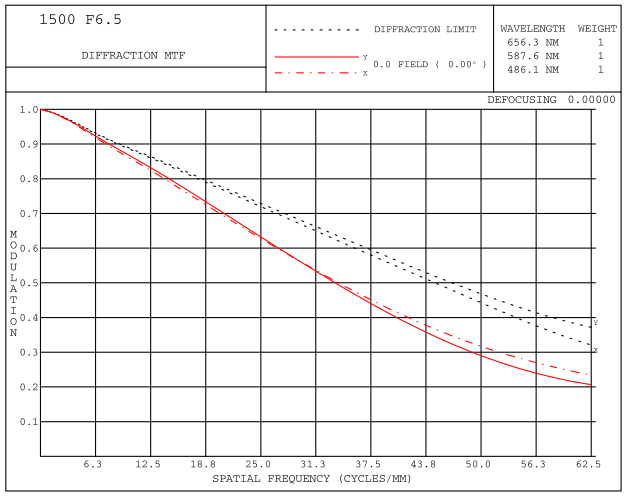

Fig. 14. MTF with low pressure.

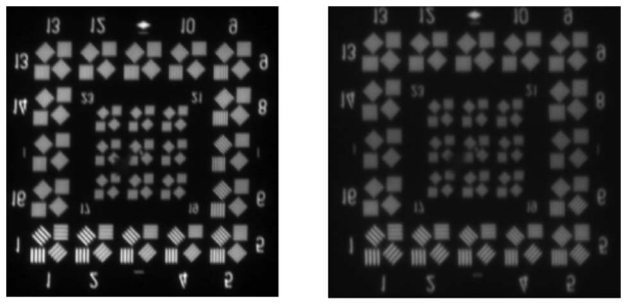

(a) At low temperatures with normal pressure

(b) At low temperatures with low pressure

Fig. 15. Images under the conditions of normal pressure and low pressure, respectively. (a) and (b) are images obtained from the same target in a low temperature environment with new thermal control devices working, under normal and low pressure, respectively. Both of them can distinguish the 5th group of stripes.

7. SUMMARY

Thermal control devices are an indispensable part of aerial remote sensors. This paper verified the importance of temperature uniformity and improved thermal control measures to ensure the temperature uniformity. The experimental results show that the modified measures are able to meet the temperature requirement of the remote sensor at both atmospheric pressure and low pressure conditions.

Funding. National Natural Science Foundation of China (NSFC) (61405192).

Acknowledgment. The authors are thankful for the support from the Key Laboratory of Airborne Optical Imaging and Measurement, Changchun Institute of Optics, Fine Mechanics and Physics, Chinese Academy of Sciences.

REFERENCES

1. C. H. Amon, J. Murthy, S. C. Yao, S. Narumanchi, C. F. Wu, and C. C. Hsieh, "MEMS-enabled thermal management of high-heat-flux devices EDIFICE: embedded droplet impingement for integrated cooling of electronics," Exp. Therm. Fluid Sci. **25**, 231–242 (2001).
2. P. M. Attia, M. R. Lewis, C. C. Bomberger, A. K. Prasad, and J. M. O. Zide, "Experimental studies of thermoelectric power generation in dynamic temperature environments," Energy **60**, 453–456 (2013).
3. J. Carlson, D. Menicucci, P. Vorobieff, A. Mammoli, and H. B. He, "Infrared imaging method for flyby assessment of solar thermal panel operation in field settings," Appl. Therm. Eng. **70**, 163–171 (2014).
4. W. L. Cheng, N. Liu, and W. F. Wu, "Studies on thermal properties and thermal control effectiveness of a new shape-stabilized phase change material with high thermal conductivity," Appl. Therm. Eng. **36**, 345–352 (2012).
5. X. B. Cheng, J. L. Zhang, T. Ding, Z. Y. Wei, H. Q. Li, and Z. S. Wang, "The effect of an electric field on the thermomechanical damage of nodular defects in dielectric multilayer coatings irradiated by nanosecond laser pulses," Light Sci. Appl. **2**, e80 (2013).
6. J. Choi, W. Sano, W. J. Zhang, Y. Yuan, Y. Lee, and D. A. Borca-Tasciuc, "Experimental investigation on sintered porous wicks for miniature loop heat pipe applications," Exp. Therm. Fluid Sci. **51**, 271–278 (2013).
7. I. Colomina and P. Molina, "Unmanned aerial systems for photogrammetry and remote sensing: a review," ISPRS J. Photogr. Remote Sens. **92**, 79–97 (2014).
8. S. Koeber, R. Palmer, M. Lauermann, W. Heni, D. L. Elder, D. Korn, M. Woessner, L. Alloatti, S. Koenig, P. C. Schindler, H. Yu, W. Bogaerts, L. R. Dalton, W. Freude, J. Leuthold, and C. Koos, "Femtojoule electro-optic modulation using a silicon-organic hybrid device," Light Sci. Appl. **4**, e255 (2015).
9. P. Liebetraut, S. Petsch, J. Liebeskind, and H. Zappe, "Elastomeric lenses with tunable astigmatism," Light Sci. Appl. **2**, e98 (2013).
10. H. Morimitsu and S. Katsura, "Control of thermal conductance of Peltier device using heat disturbance observer," Electr. Eng. Jpn. **185**, 44–52 (2013).
11. B. Saggin, M. Tarabini, and G. Lanfranchi, "A device for the skin-contact thermal resistance measurement," IEEE Trans. Instrum. Meas. **61**, 489–495 (2012).
12. S. A. Whalen and R. C. Dykhuizen, "Thermoelectric energy harvesting from diurnal heat flow in the upper soil layer," Energy Convers. Manage. **64**, 397–402 (2012).
13. K. B. Doyle, V. L. Genberg, and G. J. Michels, *Integrated Optomechanical Analysis* (SPIE, 2002), Chap. 4.
14. R. K. Banyal, B. Ravindra, and S. Chatterjee, "Opto-thermal analysis of a lightweighted mirror for solar telescope," Opt. Express **21**, 7065–7081 (2013).
15. F. P. Incropera, D. P. DeWitt, T. L. Bergman, and A. S. Lavine, *Fundamentals of Heat and Mass Transfer* (Wiley, 2011), p. 12, 401, and 435.